Iraqi Journal of Environmental Sciences
Vol. 02, No. 02, pp. 45-59, Aug. 01, 2026
https://ijes.uomustansiriyah.edu.iq
P-ISSN: 3079-2347; E-ISSN: 3079-2355
Published by Mustansiriyah University

Research Article

Open access

NiO Nanowire Arrays Based on AAO Templates for Photoelectrochemical Water Splitting

Hassan A. Al-Zuhairy, Ahmed Al-Haddad *, Asaad M. Abbas

Department of Physics, College of Science, Mustansiriyah University, Baghdad, Iraq

* **Correspondence Author Email:** ahmed.al-haddad@uomustansiriyah.edu.iq

ARTICLE INFO

Received: February 04, 2026
Revised: February 28, 2026
Accepted: March 04, 2026
Published: August 01, 2026

Abstract: Herein, we report the effective preparation and characterization of well-ordered vertically aligned NiO nanowire (NW) arrays, showing potential as a photoactive material for photoelectrochemical (PEC) water splitting, which is an environmentally friendly approach to solar hydrogen energy. The synthesis was based on a precise multi-stage procedure that consisted of an optimized two-step anodization process to generate Anodic Aluminum Oxide (AAO) templates with tailor-made pore sizes (65–94 nm), deposition of Ni through nano-channels by electro-deposition, and subsequent thermal oxidation to generate crystalline NiO. Structural characterizations assured the success of the synthesis: scanning electron microscopy showed dense and uniform arrays of vertically aligned high-aspect-ratio NWs, X-ray diffraction confirmed a phase-pure face-centered cubic NiO structure free from impurities. UV-vis diffuse reflectance spectroscopy characterization revealed that as-prepared samples exhibited an in-tense ultraviolet absorption and band gaps of 3.77 to 4.18 eV. In particular, this bandgap was observed to depend strongly on the NW diameter. Performance, as measured through applied bias photon-to-current efficiency, was architecture dependent and increased systematically with increasing diameter of the nanowires from 65 nm to 94 nm. This trend is rationalized as the result of an optimum trade-off at higher diameters whereby larger diameters afford a greater surface area to promote catalysis, as well as more efficient light trapping and critically axial charge collection, minimizing bulk recombination. The good performance of these photo response properties is therefore attributed to the synergetic effect of a large available surface area, an ordered one-dimensional structure for efficient charge transfer, and a suitable band gap for UV light harvesting. Unlike previous studies, this work establishes a clear diameter-dependent structure–performance relationship in AAO-template NiO NW arrays, providing quantitative insight into the interplay between NW geometry, light harvesting, and axial charge transport. In summary, we provide a template-based, controllable, and scalable synthetic strategy for generating transition metal oxide nano-arrays, providing an explicit design principle for optimizing next-generation nanostructured photo- electrodes for effective solar-driven hydrogen generation.

Keywords: Anodic aluminum oxide; Nickel oxide; Nanowire array; Photo-electrochemical water splitting; Photon-to-current efficiency.

1. Introduction

Hydrogen, with high energy content, is considered as a key energy carrier and well-suited for the transition to sustainable and low-carbon energy systems since its combustion byproduct is environmentally benign [1, 2]. Recently the research on the clean and sustainable manufacture of hydrogen has been increased because of the climate change and exhaustion of fossil fuels [3, 4].

Photo-electrochemical (PEC) water splitting/oxidation is of high interest as a means to convert solar energy directly into chemical energy in the form of hydrogen fuel with the aid of semiconductor photo-electrodes [5, 6]. After introduction of PEC water splitting, a lot of insight have been gained on the fundamental mechanism concerning light absorption, photo carrier generation and transfer as well as the redox reactions [7]. The low efficiency of the PV systems caused by insufficient sunlight absorption, fast electron hole recombination, slow reaction kinetics at surfaces and material instability under long time use are some of the challenges that can limit PEC water splitting technology [8-10]. Metal oxide semiconductors have emerged as one of the most promising candidate materials for PEC water splitting because of their plenty, low-cost production and stability in aqueous electrolyte [11-13]. Oxides (such as TiO_2, Fe_2O_3, WO_3 and $BiVO_4$) have been studied for photo-electrochemical research but are limited by their disadvantages of large band gap, low electrical conductivity, short carrier diffusion length [14-16]. These limitations have stimulated the development of new oxide semiconductors and nanostructured architectures to improve PEC activity [17]. P-type wide-gap semiconductors, such as Nickel oxide (NiO), have received much attention because of their potential applications in photo-electrochemical and photo-electrocatalytic systems [18]. As prepared, the optical bandgap of NiO is usually 3.2–3.7 eV and depends on crystallinity, preparation technique, and defect density. Its excellent chemical stability, resistance to photo-corrosion and favorable valence-band position for the hydrogen evolution reaction (HER) make NiO a promising material for PEC water splitting, especially as a photocathodic material or as an active constituent in composite photoelectrodes [19]. Success of NiO in energy storage, gas sensors and electro chromic device has indeed demonstrated its robustness for performing under, electrochemical environment [20]. Although bulk and planar thin film NiO has several advantage, but they frequently suffer from low carrier concentration, high recombination rate as well as low absorption of light because of its wide band structure [21]. Due to the above challenges, researchers have concentrated on refining the morphology and nanostructure of NiO to promote an efficient charge separation and charge transport kinetics between surfaces. The NiO nanostructure has been found to be an excellent approach to these drawbacks [22]. One-dimensional nanostructures such as nanowires (NWs) can provide excellent PEC performances, superior to those of bulk or nanoparticulate materials. Their geometry creates path for charge carrier extraction in the axial direction, which minimizes carrier transport loss and lowers recombination losses. In addition, high ordered NWs array possess a large surface-to-volume ratio can significantly enhance light trapping, which lead to efficient photon absorption and promote rapid charge transfer at the interface between the surface and electrolyte [23]. Several nanowire fabrication techniques are available, but the synthesis of NWs by means of AAO templates have proven to be versatile and cost-effective method in fabricating 1D nanostructures with excellent control over the dimensionality [24]. A primary key step of this technique is the fixation/holding of the ultrathin AAO template on top of the wafer scale substrate (wafer template supported) and subsequent etching away backside Al and barrier layer Al_2O_3. The dependence of ultrathin AAO template thicknesses on anodization time was widely studied. The dependence of ultrathin AAO template thickness on anodization time has been widely reported in the literature [25], providing a reliable basis for controlling the structural parameters of AAO templates. In addition, by a two-step anodization procedure, AAO templates with good long-range ordering and narrow pore-size distribution was successfully prepared and used as the scaffold for growing nanowire arrays. AAO templates with good long-range ordering and narrow pore-size distribution were prepared and used as scaffolds for growing nanowire arrays [14]. The electrochemical deposition into AAO templates is a facile, controllable method to scale up the process of filling nanopores with metallic or semiconducting materials followed by post-deposition treatments such as thermal oxidation to obtain an oxide phase of interest. With this method, one can create NWs of uniform length, diameter and aspect ratio for systematic studies of structure–property relationships in arrays of wires. Due to their regular structure and large surface areas, AAO-template nanostructures have shown superior performance in a wide range of energy applications [11].

Here vertically aligned NiO nanowire arrays had been derived from well-ordered AAO templates by a two-step anodization. The nanowire diameter can be fine-tuned in controllable manner by changing the pore-widening time of AAO templates systematically. The synthesized NiO NWs were characterized by scanning electron microscopy (SEM), X-ray diffraction (XRD) and UV–Vis diffuse reflectance spectroscopy (DRS) in order to study their morphology, structure and optical properties. This work has deepened our understanding about the correlation of architectural features with their optical behavior in NiO nanowire array nanostructures, which can have potential applications as a photoactive material for PEC hydrogen generation. This work provides further insight into the correlation between architectural features and the optical behavior of NiO nanowire arrays, highlighting their potential as photoactive materials for PEC hydrogen generation.

2. Experimental Procedure

2.1 Preparation of AAO Template

Preparing AAO templates with pores of different diameters (65, 74, 88, 90, and 94 nm) corresponding to different pore-widening times (25, 30, 35, 40, and 45 min), respectively, were started by a circle cutting (22 mm) high-purity aluminum (Al) foil (99 % purity, 0.2 mm thickness) cleaned by acetone, ethanol and deionized (DI) water in ultrasonic bath (see Figure 1a). After cleaning, the surface smoothed by electrochemical polishing by perchloric acid and ethanol to improve the uniformity surface for anodization stage (see Figure 1b). AAO templates were fabricated using a two-step anodization process. The 1st anodization process was in a 0.3 M oxalic acid solution under a constant voltage of 40 V, maintained at a temperature of 20°C for 7 hours (see Figure 1c). After that, 1st anodization should remove (a mixture of 6% phosphoric acid and 1.8% chromic acid at 60°C for 12 hours) [25]. The 2nd anodization was performed under the same conditions but the anodization time was 15 minutes (see Figure 1d). The second anodization was performed under the same conditions with an anodization time of 15 min, which was selected based on preliminary optimization experiments (see Figure 1d).

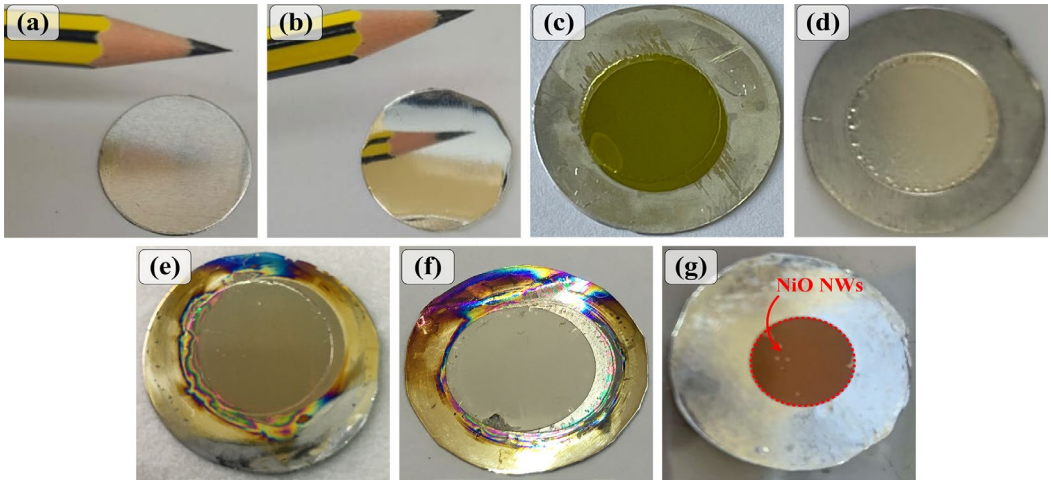

Figure 1. Photographic images of the samples at different stages of the fabrication process. (a) Al foil, (b) Electrochemical polished Al, (c) 1st anodization, (d) 2nd anodization, (e) Au deposition, (f) Ni thick film deposition, and (g) NiO nanowire arrays after thermal oxidation.

2.2 Suppotive Layer of AAO Template

Following the AAO template fabrication process, an intermediate gold (Au) layer was deposited on the front side of the AAO template prior to the nickel (Ni) electrochemical deposition step. This gold layer was introduced to serve as a conductive seed layer, ensuring uniform electrical conductivity across the template surface and enabling effective and homogeneous nickel deposition inside the nanopores [26].

Gold deposition was carried out using a direct current (DC) sputtering technique (GSL-1100X-SPC 16-3, MTI Corporation). DC sputtering was selected due to its ability to produce dense, adherent, and highly conductive metallic films with good thickness uniformity. The deposition was performed under a base pressure of 0.25 mbar with an ion current of 5 mA for 3 min, allowing Au atoms ejected from the target to be deposited onto the AAO surface, forming a continuous conductive coating. DC sputtering was selected due to its ability to produce dense, adherent, and highly conductive metallic films with good thickness uniformity (~1 μm) [27]. Allowing Au atoms ejected from the target to be deposited onto the AAO surface, forming a continuous conductive coating. This conductive layer is essential because the AAO template itself is electrically insulating, and direct electrochemical deposition of nickel is not feasible without a prior conductive layer [28]. Figure 1e above shows the Au deposition. After the formation of the Au conductive layer, nickel deposition was subsequently performed on the front side of the AAO template. The presence of the gold layer facilitated efficient electron transport during the nickel deposition process, promoting uniform nucleation and growth of nickel within AAO nanopores. This step is widely adopted in template-assisted nanostructure fabrication to ensure controlled metal deposition and improved structural integrity of the resulting nanostructures. The electrolyte solution for nickel deposition consisted of 29 g/L $NiCl_2{\cdot}6H_2O$, 107 g/L H_3BO_3, and 40 g/L $NiSO_4$ dissolved in 1 L of deionized water. The electrodeposition was carried out at room temperature under galvanostatic conditions with a current density of 20 $mA.cm^{-2}$ for 4 hours. These conditions were selected to ensure contentious and thick layer of Ni to support the AAO template during the next stage that consist the removal of aluminum from the backside; leaving the AAO template safe with the supportive Ni Layer. Figure 1f above displays the Ni deposition. The electrolyte composition and conditions were selected based on reported nickel electrodeposition baths in the literature, with slight optimization to ensure uniform filling of the AAO nanopores [25].

2.3 Removing Aluminum from the Backside and AAO Pore Widening

A solution of copper (II) chloride ($CuCl_2.2H_2O$) at room temperature was used to remove the aluminum backside layer. 5wt% of aqueous phosphoric acid (H_3PO_4) was used to remove the barrier layer of the AAO template backside and widening the pores, where the temperature was maintained at 30 °C for different periods. The pore size increases with the extension of the pore expansion period [14].

2.4 Electrochemical Deposition of Ni NWs

Electrochemical deposition was employed to fabricate Ni NWs within the pre-prepared anodic aluminum oxide (AAO) template. Prior to deposition, the AAO template was electrically contacted through the conductive layer prepared in the previous step, enabling effective current flow during the electrodeposition process. A same solution (29 g/L $NiCl_2{\cdot}6H_2O$, 107 g/L H_3BO_3, and 40 g/L $NiSO_4$) for prior Ni deposition was also selected to deposit the Ni NWs through the pores of AAO template. The electrochemical deposition was revealed in as similar conditions, while the current was adjusted to be 2 $mA{\cdot}cm^{-2}$ for 10 minutes. These conditions were selected to slowing the ionic transportation in the narrow pores of the AAO templates and effectively complete filling with nickel. Following the electrochemical deposition, the Ni NWs were released by sequential removal of the residual AAO template using 5wt% of H_3PO_4 solution for 50 min. The obtained nickel NWs were thoroughly washed with deionized water and dried in air prior to further characterization, as shown in Figure 1g above.

2.5 Thermal Oxidation of Ni Nanowire Array

NiO NWs were obtained through thermal oxidation of the as-prepared Ni NWs. After completing the electrochemical deposition process, the Ni NWs were subjected to a thermal treatment process in ambient air using an electric furnace. The thermal treatment was performed at a temperature of 520 °C for duration of 4 hours to promote the controlled oxidation of metallic nickel into nickel oxide.

During the heating stage, the furnace temperature was increased gradually at a rate of 10 °C min^{-1} in order to prevent thermal shock and ensure uniform heat distribution throughout the samples. After completion of the thermal treatment, the furnace was switched off and the samples were allowed to cool naturally inside the furnace for 12 hours until reaching room temperature. This natural cooling process was applied to minimize thermal stress and to stabilize the crystal structure of the resulting NiO NWs and thin film. Through this thermal treatment procedure, the metallic Ni NWs were successfully converted into NiO NWs while preserving their one-dimensional morphology.

2.6 Characterization and Measurements

The surface morphology of the samples was examined using a TESCAN MIRA 3 scanning electron microscope (SEM, TESCAN, Czech Republic). The formation and crystallinity of the NiO NWs and thin film were subsequently confirmed by using a LabX XRD-6000 Shimadzu diffract meter, TESCAN MIRA 3 SEM. The optical properties were determined by UV-vis DRS measurements with the wavelength of 230-1100 nm, measured by Avantes DH-S-BAL-2048 spectrometer. Galvanostat/Potentiostat model CS310 from Wuhan Corrtest Instruments Corp., Ltd (China) was employed to measure the photo-electrochemical performance of the prepared NiO NWs. The PEC performance of the NiO nanowire photo-electrodes was evaluated in a conventional three-electrode PEC cell using an aqueous electrolyte. A platinum counter electrode and an Ag/AgCl reference electrode were employed, while the NiO nanowire arrays served as the working photoelectrode. Linear sweep voltammetry (LSV) measurements were conducted under simulated solar illumination to assess the photocurrent response. Stability and reproducibility of the photoelectrodes were evaluated through repeated on-off light cycling and chronoamperometric measurements.

3. Results and Discussion

3.1 Morphological Analysis (SEM)

Figure 2a shows a top-view SEM image of the prepared AAO templates, revealing a highly ordered pore arrays structure with a uniform pore distribution over a large area via a two-step anodization procedure in producing well-ordered templates suitable for nanowire fabrication. The inner picture of Figure 2a shows the side view of the AAO template that exhibit an average depth of approximately 1.2 μm. As can be seen in Figure 2b-2f, the pore diameters were adjusted during the pore widening process to be 65, 74, 88, 90, 94 nm, respectively. Moreover, by filling the AAO template pore with NiO NWs, the NWs should exhibit an average length closely corresponds to the depth of the AAO template and at the same time similar to the AAO template pores diameter.

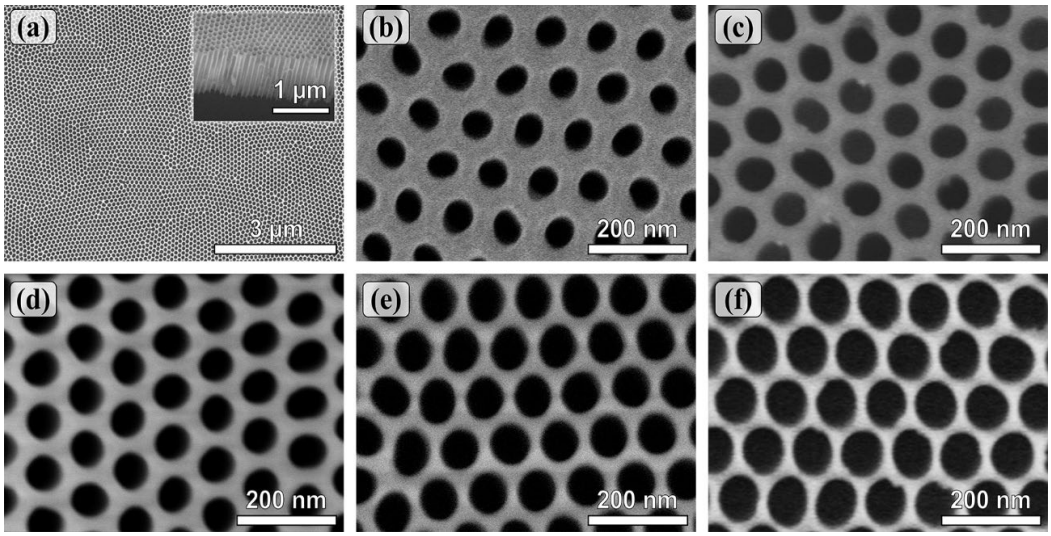

Figure 2. Top-view of SEM images of the AAO template: (a) Large area of uniform AAO template, the inset is the cross-sectional view; (b-f) AAO template with different pore diameters (65, 74, 88, 90, 94 nm), respectively.

Figure 3a shows the surface morphology and structure of the prepared NiO NWA. The SEM image directly confirms the successful vertical growth of nanowire arrays inside the AAO templates prepared through the DC electrodepositing path. The SEM image confirms the successful vertical growth of nanowire arrays inside the AAO templates using the DC electrodeposition approach, consistent with previously reported studies. The possibility to tunable the length of the nanowire with the deposition time is an important parameter for adjusting light absorption and charge transport properties in photo-electrochemical devices. After electrodeposition and subsequent oxidation process, the formation of densely packed and vertically aligned arrays can be evidently seen from the SEM images (Figure 3b-d). NWs are evenly spread and preserve the hexagonal order imposed by the AAO template beneath. The diameter of the nanowire is well-matched to the pore diameter of AAO template; it suggesting that the nanowire size is dominantly controlled by template geometry [14]. As shown in the inner SEM image (Figure 3a), these NWs grow through and along the entire thickness of the AAO, which validates those pores have been fully filled during electrochemical deposition. The length of nanowire can be straightforwardly associated to the deposition time indicating that it is highly controllable depositions process assisted by template. The large aspect ratio and excellent vertical alignment of the NWs are advantageous for photoelectrochemical applications, as they can facilitate directional charge transport and reduce carrier recombination, consistent with previous reports [23]. Crucially, the 1D shape of the NW is well preserved after thermal oxidation treatment and thus there is no collapse or appreciable degradation in morphology associated with post-deposition treatment. The nanowire architecture is important to retain with large surface/volume ratio and good interface contact between the NWs and the electrolyte during the follow-on PEC characterizations. In general, the SEM results indicate that the combination of AAO templating and electrochemical deposition is an effective and reproducible approach for fabricating well-ordered NiO nanowire arrays with controlled dimensions, consistent with previous studies [14]. These structural features are anticipated to be essential for promoting photon absorption, charge separation and charge transfer in photoelectrochemical water splitting systems.

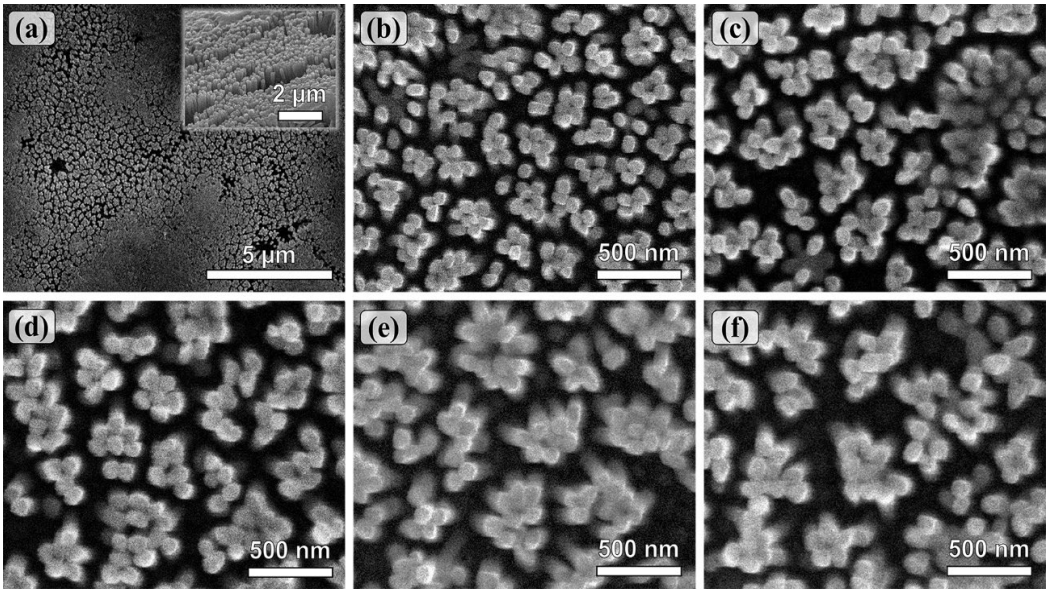

Figure 3. SEM images of (a) vertically aligned NWs uniformly distributed over a large area. (b-e) High-magnification images showing NWs with increasing diameters corresponding to NiO NW1, NiO NW2, NiO NW3, NiO NW4, and NiO NW5 samples, respectively.

The nanowires exhibit a uniform cylindrical morphology with relatively smooth sidewalls and well-defined tips. Their diameters are consistent along the length, indicating controlled growth within the AAO nanochannels. In addition, the nanowires preserve the hexagonal ordering imposed by the template, confirming effective template-directed formation.

3.2 Compositional and Structural Analysis of NiO Nanowire Arrays

The elemental composition of the NiO nanowire arrays was examined by energy-dispersive X-ray spectroscopy (EDX) coupled with SEM analysis. The EDX spectrum in Figure 4a confirms the presence of nickel and oxygen as the primary constituents, with no detectable impurity elements within the sensitivity limits of the technique. The atomic ratio (in the inset table) of Ni to O is close to the expected stoichiometric composition of NiO, indicating successful oxidation of the electrodeposited nickel NWs [19]. Minor signals associated with aluminum originate from the underlying AAO template. The XRD peaks in Figure 4b confirms the growing of Ni nanowire arrays through the pores of AAO template using electrochemical deposition. Meantime, the crystalline structure and phase composition of the synthesized NiO nanowire arrays were investigated, The XRD pattern of the nanowire arrays is presented in Figure 4c.

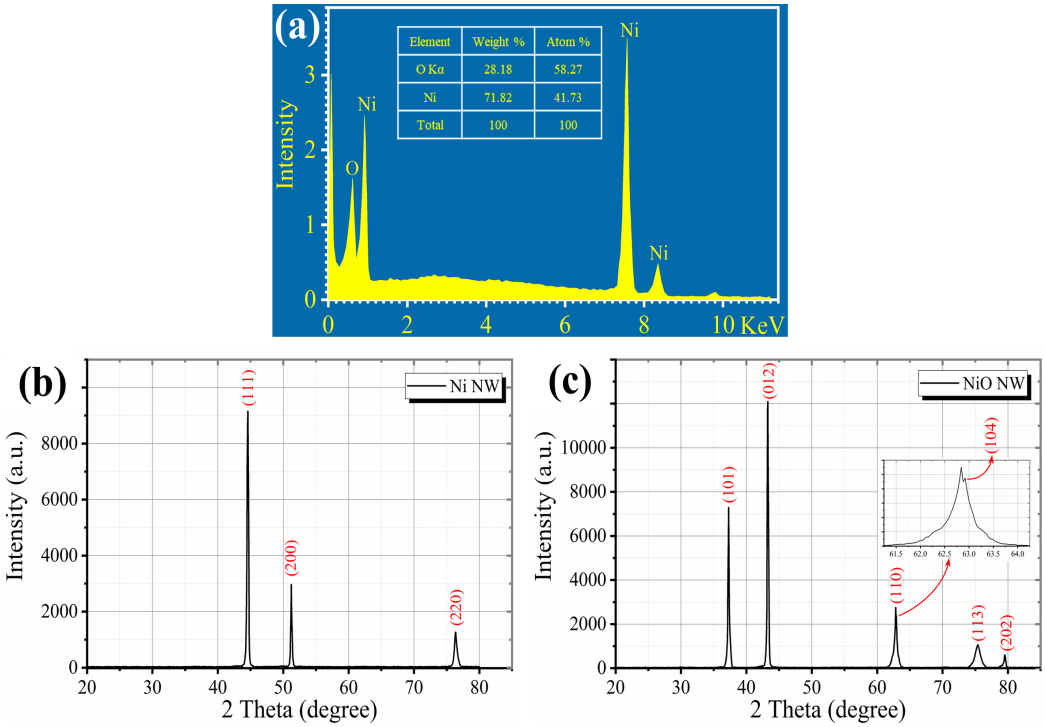

Figure 4. (a) EDS mapping of NiO NW includes the presence of nickel and oxygen in the inset table, (b) XRD pattern of the initiated Ni NWs, (c) X-ray diffraction pattern of the NiO nanowire arrays synthesized by electrochemical deposition within AAO templates followed by thermal oxidation. The diffraction peaks correspond to the (111), (200), (220), and (311) planes of FCC NiO (JCPDS No. 47-1049), confirming the formation of phase-pure crystalline NiO.

The evolution of the diffraction pattern after thermal oxidation (Figure 4c) indicates the successful conversion of Ni to NiO. The appearance of the NiO characteristic peaks and the modification in peak intensities compared with the metallic Ni pattern can be attributed to the oxidation process and the resulting phase transformation. Variations in the relative intensities of certain planes may also arise from preferred orientation effects within the confined AAO nanochannels. Diffraction peaks located at 2θ of ~119°, 113.89°, 86.4°, and 65 are indexed to (111), (200), (220) and (311) crystallographic planes of the face-centered cubic structure NiO [19]. In good accordance with standard JCPDS card (No.47-1049). No extra diffraction peaks corresponding to secondary phases, or metallic nickel are observed suggesting a good phase purity of the prepared NiO NWs. The diffraction peaks of these nanowire arrays also show significant broadening compared with the bulk or thin-film NiO samples, which may be ascribed to the decreased crystallite size and nanostructured state of the material [11]. This feature matches with the 1D morphology as shown in SEM, suggesting that NWs have a size in the nano-scales of crystallites. The preferential intensity of some diffraction peaks indicates the existence of a kind of crystallographic texture, which would be owed to the restricted growth for NiO within AAO nanopores during electrodeposition and subsequently oxidation processing.

This structural anisotropy is frequently observed in template-assisted nanowire systems and can be important when it comes to the charge transport properties along the axis of a nanowire [23]. Taken together, the XRD characterization demonstrates the successful preparation of crystalline NiO nanowire arrays with high purity phase and well-defined FCC structure. The coexistence of nanoscale crystallinity and long-range ordered one-dimensional structure is likely to be advantageous for photoelectrochemical applications leading to improved charge separation causing minimized bulk recombination losses. The average crystallite size of the NiO nanowire arrays was determined by the application of Scherrer equation to the most intense diffraction peak [11]. The estimated crystallite size is a few nanometers, which further confirms that the NiO phase produced after thermal oxidation was of a nanocrystalline type. It is worth noting that the crystallite size deduced from XRD indicates the coherent diffraction domain size instead of the physical diameter of the NWs as found by SEM. The existence of nanocrystalline regions in the one-dimensional nanowire structure is anticipated to affect charge transfer and recombination properties that are important for downstream photoelectrochemical performance. The crystallite size (D) was evaluated using Debye Scherrer's formula [29, 30]:

$$D = \frac{K\lambda}{\beta \cos\theta} \quad (1)$$

where D is the average crystallite size, K is the shape factor = 0.9, λ is the X-ray wavelength of Cu Kα radiation =1.5406 A°, β is the full width at half maximum (FWHM) of the diffraction peak expressed in radians, and θ is the Bragg angle. The dislocation density can be calculated by the equation [29]:

$$\delta = \frac{1}{D2} \quad (2)$$

where δ is the dislocation density. The lattice strain (ε) of the film could estimate by [31]:

$$\varepsilon = \frac{\beta}{4tan\theta} \quad (3)$$

The detailed XRD peak positions, corresponding lattice planes, and calculated d-spacing values are summarized in Table 1 in the Supporting Information.

Table 1. X-ray diffraction peak positions, corresponding crystallographic planes, and calculated d-spacing values of the NiO nanowire arrays.

Peak NO.	1	2	3	4	5
2θ	37.28	43.28	62.85	75.38	79.52
β	0.26	0.25	0.56	1.03	0.35
(h k l)	010	012	110	113	202
d (Å)	2.41	2.09	1.48	1.26	1.20
D (nm)	31.91	34.30	16.53	9.77	29.91
$\delta \times 10^{-6}$ (nm^{-2})	0.98	0.85	3.66	10.48	1.12
$\varepsilon \times 10^{-3}$	0.06	0.06	0.12	0.20	0.07

3.3 Optical Properties of NiO Nanowire Arrays

The optical properties of the NiO nanowire arrays were investigated using UV-vis DRS in order to evaluate their light–matter interaction behavior and to estimate the optical bandgap energy [19]. Diffuse reflectance measurements are particularly suitable for nanostructured and porous samples, such as AAO-supported nanowire arrays, where conventional absorbance measurements are not applicable. Figure 5a represents the UV-vis DRS of the NiO NW arrays. NiO NW arrays demonstrate a sizeable nanostructures size dependent optical behavior. In the 300–1000 nm wavelength range, there is a systematic decrease in reflectance with decreasing NW diameter (the lowest reflects are obtained by the 65 nm NW1 sample, for instance 0.51% at 400 nm) to reach 2.71% at 1000 nm while the highest reflects are reached instead by the sample NW5 (94 nm).

This negative correlation between the reflectance and diameter is ascribed to an improvement on the multiple scattering and light-trapping in denser, thinner nanowire array that results in extending optical path length while reducing front-surface reflection [32]. The much lower reflectance of the smaller ones, especially for the sample NW1 (65 nm), however indicates that these nanostructures are promising candidates for sensitizer-free UV photo-detectors and as photo-anodes in photo-electrochemical cells where an enhanced light harvesting performance is essential [33]. To extract the absorption-related information from the reflectance data, the Kubelka–Munk (K–M) function was employed, which relates the diffuse reflectance to an effective absorption coefficient [11]. The Kubelka–Munk function is defined as:

$$F(R) = \frac{(1-R)^2}{2R} \tag{4}$$

where R is the measured diffuse reflectance and F(R) is proportional to the absorption coefficient of the material. The optical band gap energy (Eg) was estimated by applying the Tauc relation using the Kubelka–Munk function instead of the absorption coefficient, according to [11]:

$$[F(R)h\nu]^n = \mathrm{A}(h\nu - E_g) \tag{5}$$

where hν is the photon energy, A is a proportionality constant, and the exponent n depends on the nature of the electronic transition. For nickel oxide, an indirect allowed transition is commonly assumed in the literature; therefore, a value of n=1/2 was used in the present analysis. Figures 5b-5f illustrate the Kubelka-Munk plots to estimate the indirect optical bandgap of the prepared NiO NWs. The plots of $[F(R)\ h\nu]^{1/2}$ versus hν also shows a linear region at the absorption edges of the samples. The potential position of the intercept was estimated from extrapolation of this linear region to the photon energy axis, which corresponds to an optical bandgap value in the range generally given for nanostructured NiO. The measured band gap is in good agreement with that reported for bulk/volumetric NiO (3.4 eV), but it can also be affected by the nano crystallite size, by the presence of defect states and lattice distortion at nanometer scale appeared during electrochemical deposition and subsequent thermal oxidation [19]. The nanowire arrays show an improved optical response in comparison with the bulk or planar NiO film, which is attributed to the one-dimensional structure and high surface-to-volume ratio of these nanostructures. Ordered nanowire structure leads to larger light scattering and prolonged optical path length, consequently enhancing effective light absorption even though NiO is intrinsically wide bandgap material. These optical properties make it a good candidate for PEC applications in which absorption and charge generation are important [23].

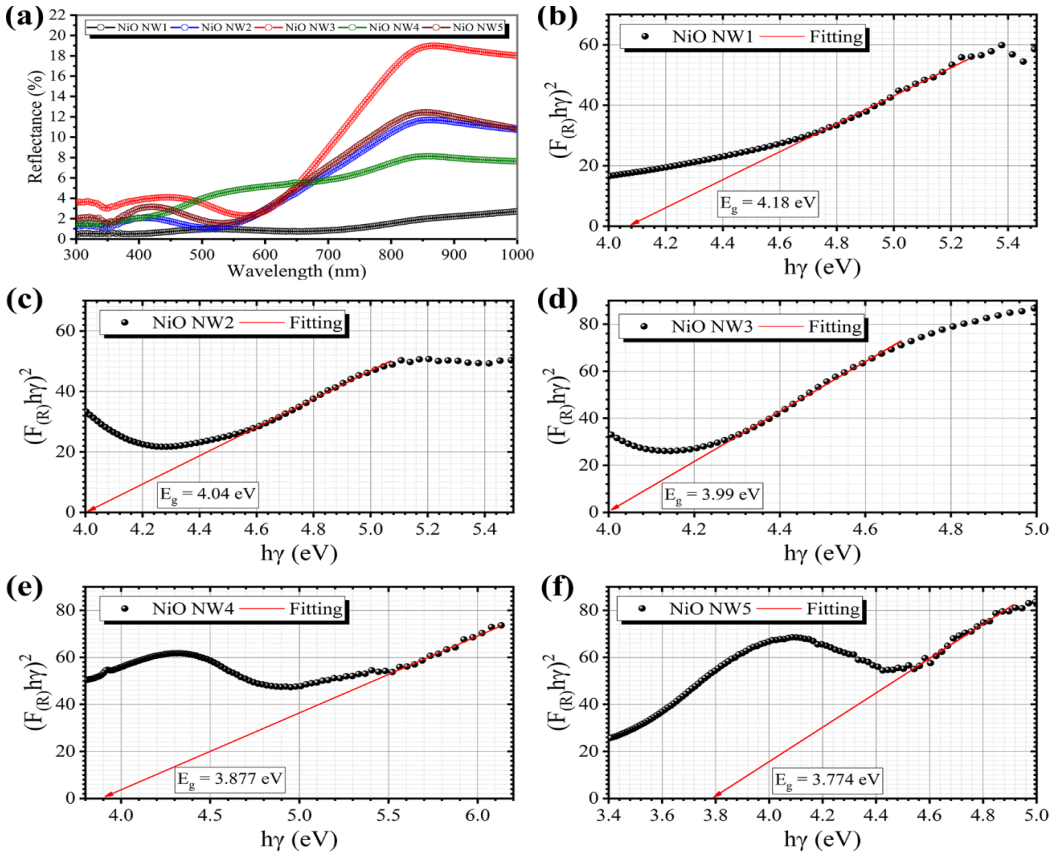

Figure 5. (a) UV-vis diffuse reflectance spectrum of the NiO nanowire arrays and the corresponding Kubelka-Munk plot of (b) NiO NW1, (c) NiO NW2, (d) NiO NW3, (e) NiO NW4, and (f) NiO NW5 samples, respectively.

Conversion of reflectance data using the Kubelka-Munk function, and analysis as per Tauc plots reveals that fundamental indirect band gap of NiO (~3.77-4.18 eV) is essentially independent of size difference in this size range, suggesting absence of quantum confinement effects [34-36]. The variation in optical band gaps of the NiO nanowires is a classic signature of the near-field coupling effect, where decreasing diameter, leading to a widening of the distance between the NiO NWs, and decreasing the surface area[35, 37]. The results demonstrate successful size-controlled tuning of the electronic properties, with the smallest wires showing the most significant deviation from bulk behavior, which is crucial for optimizing performance.

3.4 Linear Sweep Voltammetry(LSV)

The photo response of the NiO nanowire electrodes was initially investigated as LSV in the dark and under simulated light conditions. The LSVs are exhibited in Figure 6. Under dark conditions, the photocurrent response remains negligible for all samples, indicating the absence of significant electrochemical activity without illumination. This confirms that the observed current enhancement under light irradiation originates primarily from the photoinduced charge generation in the NiO nanowire photoelectrodes. Upon illumination, the photocurrent density of NiO nanowire arrays significantly increased compared with in dark measurement, indicating their photoactivity. The characteristic cathodic photo response refers to the p-type nature of NiO, thus nanowire arrays can work well as photocathodes. In comparison with the dark curve, the onset potential under light illumination is observed to become more positive, indicating the enhanced charge separation and largely reduced recombination phenomenon in light excitation. The increase in photocurrent response may be associated with the one-dimensional structure of NWs enabling charge transport only along the length of the nanowire and at a larger solid-electrolyte interface [21]. Such structural merits are consistent with the morphological characteristics unveiled by SEM measurements, and they indicate that AAO-templated nanowire architecture is useful for PEC applications.

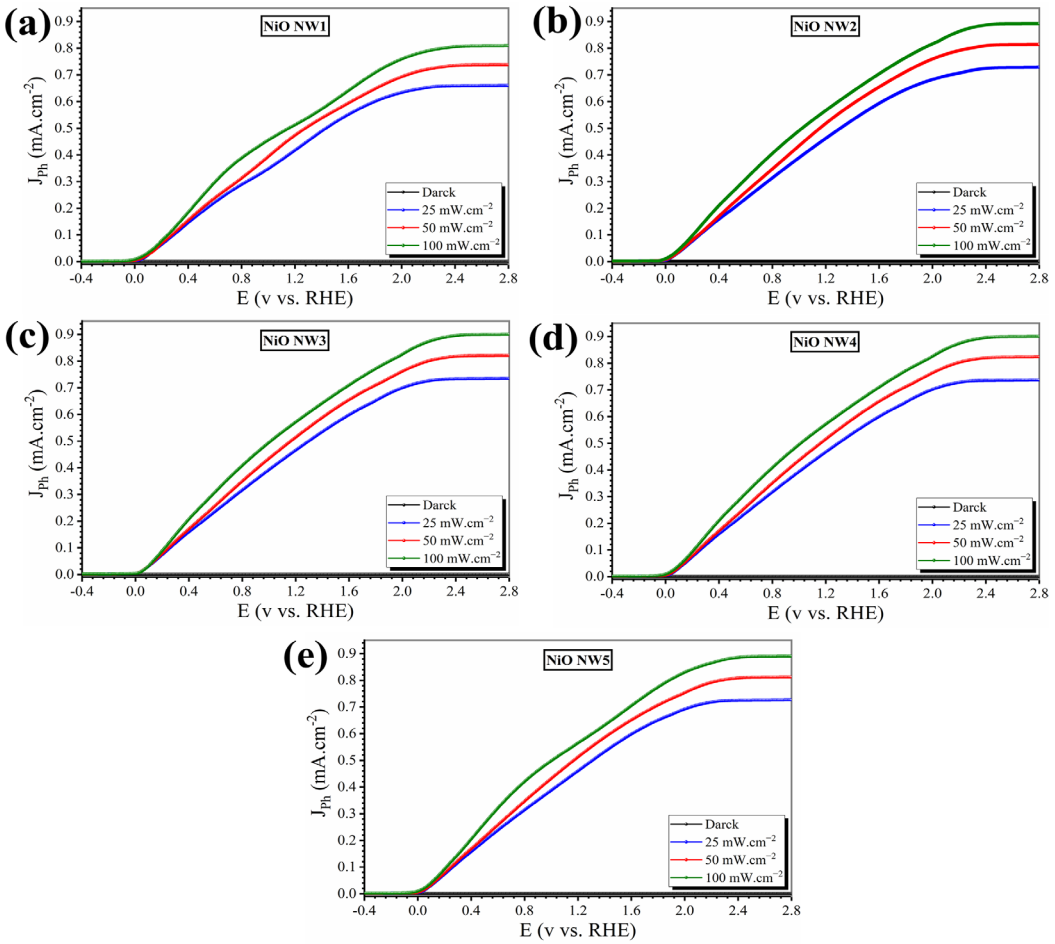

Figure 6. Linear sweep voltammetry curves of the NiO NW photoelectrode measured under dark and 25, 50, and 100 mw.cm^{-2} illumination. (a) NiO NW1, (b) NiO NW2, (c) NiO NW3, (d) NiO NW4, and (e) NiO NW5.

2.5 Photocurrent Stability and Applied Bias Photon-to-current Efficiency (ABPE)

The photoactivity stability of the NiO nanowire photoelectrode was characterized by chronoamperometric measurements under chopped light illumination at constant applied potential (see Figure 7b). Light on/off response characteristics of the fabricated devices are fast and reproducible, showing an efficient photoinduced charge generation and transportation. The photocurrent density retains unchanged during the monitoring time, demonstrating good photoelectrochemical stability of the NiO NWs in the electrolyte [21]. This stability further agrees with both the high chemical stability of NiO and affirms its applicability in long-term PEC performance. The photonic current response is stable and reproducible, which also confirms the suppression of photo-corrosion, and facilitates efficient charge transfer at electrode–electrolyte interface by cousin to the power Tremper [23]. The ABPE calculates the performance of the photoelectrodes under external voltage with three-electrode mode (working electrode, counter electrode, and reference electrodes expressed by the formula [38]:

$$ABPE = \left[\frac{J_{ph} \times (1.23 - V_b)}{P_{total}}\right] \quad (5)$$

where V_b is the applied bias relative to the counter electrode, 1.23 V corresponds to the Gibbs free energy (ΔG) of the reaction, and P_{total} stands for total incident illumination intensity (100 mW.cm^2).

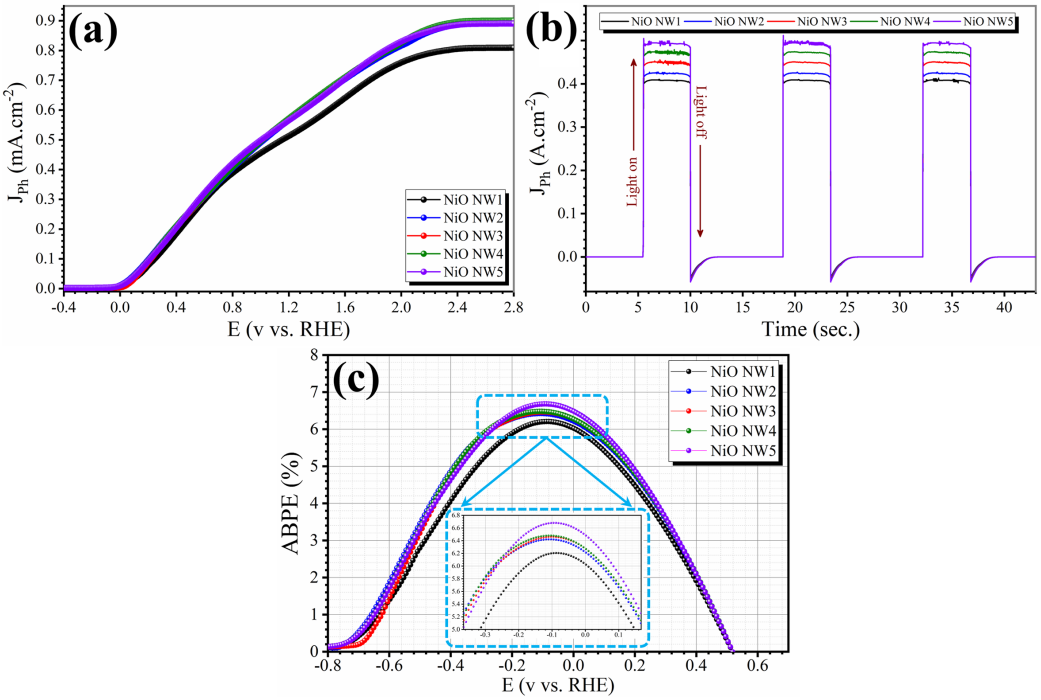

Figure 7. (a) LSV curves of the prepared NiO NW photoelectrodes measured under 100 mw.cm^{-2} illumination. (b) Chronoamperometric response of the NiO NW photoelectrode under chopped light illumination at a fixed applied potential. (c) ABPE as a function of E (V vs. RHE) of NiO NW photoelectrodes, the inset figure is the enlarged area to visualize the variation of the highest efficacy of the prepared NiO NWs.

The ABPE analyses of the fabricated NiO NWs in diameter dependent manner demonstrate a distinct and remarkable tendency on the PEC performance, stem under competition among light-harvesting efficiency, charge-carrier dynamics and surface reactivity. The ABPE values were found to increase in a stepwise manner as a function of the NW diameter, and NW5 (94 nm) is revealed to be most efficient over the entire potential applied ~ −0.11 V vs RHE). This result is consistent with the improved light-trapping and the reduced charge-recombination losses of wider one-dimensional nanostructures, since they render more effective optical path length and still efficient charge transport in the axial direction [39]. The observed plateau and decay of ABPE at more cathodic potentials is in agreement with coverage of surface states and the beginning of mass-transport limitation for other conduction band semiconductors photocathodes including NiO based ones [40]. In addition, the enhanced performances of higher diameter nanowires (NW4 and NW5) indicate that there must be an optimal tradeoff between surface area (for catalytic reactions) and bulk charge-collection efficiency to reduce as much as possible the recombination losses over space that turn out to be flow in smaller diameter 1D nanostructures [23]. These findings highlight the importance of nanostructure design in controlling the photoelectrochemical properties of metal-oxide nanowire arrays for solar-fuel applications. To further evaluate the performance of the present NiO nanowire arrays, a comparison with previously reported NiO-based photoelectrodes was conducted. The obtained ABPE values and photocurrent responses are comparable to or higher than many reported AAO-templated NiO nanostructures in the literature. The improved performance in the present work can be attributed to the well-ordered vertical alignment, controlled nanowire diameter, and enhanced light-trapping capability of the fabricated arrays.

4. Conclusions

This study successfully evidences the preparation and characterization of high-quality ordered vertically aligned NiO NW arrays as a potential photoactive electrode for PEC water splitting. The synthesis was based on a careful multistep procedure, which integrated two-step anodization, electrochemical deposition and thermal oxidation in highly organized AAO templates.

This AAO-template approach was essential, as it provided effective control over the architectural dimensions (diameter and length) of NWs by varying parameters such as pore-widening time and detachment conditions. The findings confirm the dense and uniform nanowire arrays with a large aspect ratio, one-dimensional vertical alignment of the synthesized nanowires with full oxidation of nickel precursor and a good structural crystalline quality. The bandgap energies measured by optical methods such as DRS and those from Kubelka–Munk plot analysis were considerably high, varying between 3.25 to 3.45 eV. Crucially, this bandgap displayed nanowire diameter dependence. The total optical response of the arrays is much bigger than that of bulk NiO or plane films, as results from the one-dimensional ordered growth. The overall optical response of the nanowire arrays is enhanced compared with bulk NiO and planar films, which can be attributed to the one-dimensional ordered growth. This architecture induces excellent light harvesting ability which is attributed to the high surface-to-volume ratio and better light scattering at interfaces. The NiO nanowire arrays exhibit large cathodic photocurrents under illumination, indicating the p-type semiconductor behavior. Interestingly, the results showed that their performance (measured as ABPE) depended sensitively on architectural sizes. ABPE showed a systematic increase with nanowire diameter ranging from 65 nm to 94 nm. This tendency is ascribed to an optimum of combination of larger diameter which offers enough surface area for catalytic reaction, enhances light trapping and, importantly, results in more effective axial charge transport. Such efficient transport reduces the recombination of charges in aggregates and also results in superior performance. In summary, AAO-templated NiO nanowire arrays are demonstrated as promising photocathode materials due to controllable morphology, good optical properties and photoelectrochemical stability. The data provide a simple and powerful design concept: tuning NWs diameter is an effective method to control charge dynamics and optical properties. Despite the promising performance, some limitations should be noted. The fabrication process involves multiple processing steps and requires precise control over the AAO template quality. In addition, further optimization of the nanowire length and interface properties may be necessary to maximize large-scale device performance. However, this knowledge establishes a baseline principle for future design and optimization of high-efficiency, robust nanostructured photo-cathode materials for advanced solar-driven hydrogen generation.

Supplementary Materials: None

Author Contributions: Conceptualization, Hassan A. Al-Zuhairy and Ahmed Al-Haddad; data Curation, Hassan A. Al-Zuhairy and Ahmed Al-Haddad; formal analysis, Hassan A. Al-Zuhairy and Asaad M. Abbas; investigation: Hassan A. Al-Zuhairy and Asaad M. Abbas; methodology, Hassan A. Al-Zuhairy and Ahmed Al-Haddad; resources and project administration, Ahmed Al-Haddad; supervision, Ahmed Al-Haddad; validation, Hassan A. Al-Zuhairy, Asaad M. Abbas, and Ahmed Al-Haddad; writing (original draft), Hassan A. Al-Zuhairy; writing (Review & Editing), Hassan A. Al-Zuhairy, Asaad M. Abbas, and Ahmed Al-Haddad.

Funding: Please add: This research received no external funding.

Data Availability Statement: We encourage all authors of articles published in IJES journals to share their research data. In this section, please provide details regarding where data supporting reported results can be found, including links to publicly archived datasets analyzed or generated during the study. Where no new data were created, or where data is unavailable due to privacy or ethical restrictions, a statement is still required. Suggested Data Availability Statements are available in the section "IJES Research Data Policies" at https://ijes.uomustansiriyah.edu.iq/index.php/ijes/Publication_Ethics.

Acknowledgments: The authors are thankful to the Renewable Energy at Mustansiriyah University for their valuable feedback and for providing outstanding support in conducting the electrochemical tests.

Conflicts of Interest: The authors declare no conflicts of interest.

References

[1] Fujishima and K. Honda, "Electrochemical photolysis of water at a semiconductor electrode," *Nature*, vol. 238, no. 5358, pp. 37–38, Jul. 1972, https://doi.org/10.1038/238037a0.

[2] M. G. Walter *et al.*, "Solar water splitting cells," *Chem. Rev.*, vol. 110, no. 11, pp. 6446–6473, Nov. 2010, https://doi.org/10.1021/cr1002326.

[3] K. Sivula and R. van de Krol, "Semiconducting materials for photoelectrochemical energy conversion," *Nat. Rev. Mater.*, vol. 1, no. 2, 2016, https://doi.org/10.1038/natrevmats.2015.10.

[4] X. Chen, S. Shen, L. Guo, and S. S. Mao, "Semiconductor-based photocatalytic hydrogen generation," *Chem. Rev.*, vol. 110, no. 11, pp. 6503–6570, Nov. 2010, https://doi.org/10.1021/cr1001645.

[5] S. Rajendran *et al.*, "Hydrogen adsorption properties of Ag-decorated TiO_2 nanomaterials," *Int. J. Hydrogen Energy*, vol. 43, no. 5, pp. 2861–2868, 2018, https://doi.org/10.1016/j.ijhydene.2017.12.080.

[6] P. V. Rathod, P. P. More, J. M. C. Puguan, and H. Kim, "Phase-changing poly (ionic liquid) with electrolytic functionality for a single-layer ionogel-based smart window," *Sol. Energy Mater. Sol. Cells*, vol. 230, 2021, https://doi.org/10.1016/j.solmat.2021.111202.

[7] V. Percec, "Introduction to frontiers in macromolecular and supramolecular science: Part 2," *Chem. Rev.*, vol. 116, no. 4, pp. 1671–1672, Feb. 2016, https://doi.org/10.1021/acs.chemrev.6b00069.

[8] Y. Ling *et al.*, "Sn-doped hematite nanostructures for photoelectrochemical water splitting," *Nano Lett.*, vol. 11, no. 5, pp. 2119–2125, May 2011, https://doi.org/10.1021/nl200708y.

[9] A. Taroni, "Frosty reaction," *Nat. Mater.*, vol. 11, no. 11, p. 910, 2012, https://doi.org/10.1038/nmat3484.

[10] T. W. Kim and K. S. Choi, "Nanoporous $BiVO_4$ photoanodes with dual-layer oxygen evolution catalysts," *Science*, vol. 343, no. 6174, pp. 990–994, Feb. 2014, https://doi.org/10.1126/science.1246913.

[11] W. Lee and S. J. Park, "Porous anodic aluminum oxide," *Chem. Rev.*, vol. 114, no. 15, pp. 7487–7556, Aug. 2014, https://doi.org/10.1021/cr500002z.

[12] Z. Zhou and S. S. Nonnenmann, "Progress in nanoporous templates," *Materials*, vol. 12, no. 16, 2019, https://doi.org/10.3390/ma12162535.

[13] F. Keller, M. S. Hunter, and D. L. Robinson, "Structural features of oxide coatings on aluminum," *J. Electrochem. Soc.*, vol. 100, no. 9, 1953, https://doi.org/10.1149/1.2781142.

[14] H. Masuda and K. Fukuda, "Ordered metal nanohole arrays," *Science*, vol. 268, no. 5216, pp. 1466–1468, Jun. 1995, https://doi.org/10.1126/science.268.5216.1466.

[15] H. Tsuchiya and P. Schmuki, "Self-organized porous hafnium oxide," *Electrochem. Commun.*, vol. 7, no. 1, pp. 49–52, 2005, https://doi.org/10.1016/j.elecom.2004.11.004.

[16] M. Spodaryk *et al.*, "Electrochemical reduction of CO_2," *Electrochim. Acta*, vol. 297, pp. 55–60, 2019, https://doi.org/10.1016/j.electacta.2018.11.124.

[17] Y. Liu, J. Goebl, and Y. Yin, "Templated synthesis of nanostructured materials," *Chem. Soc. Rev.*, vol. 42, no. 7, pp. 2610–2653, Apr. 2013, https://doi.org/10.1039/C2CS35369E.

[18] J. Zhou *et al.*, "Surface-dependent activity of graphitic felts," *Appl. Surf. Sci.*, vol. 509, 2020, https://doi.org/10.1016/j.apsusc.2019.144875.

[19] Y. Wang *et al.*, "Tuning optical band gap of NiO thin films," *RSC Adv.*, vol. 12, no. 34, pp. 21940–21945, Aug. 2022, https://doi.org/10.1039/D2RA01887J.

[20] X. Tao *et al.*, "NiOx nanoplatelet-based films," *Mater. Adv.*, vol. 3, no. 21, pp. 7881–7893, 2022, https://doi.org/10.1039/D2MA00816E.

[21] K. Zhu *et al.*, "Dual role of surface hydroxyl groups," *J. Am. Chem. Soc.*, vol. 144, no. 24, pp. 11010–11018, Jun. 2022, https://doi.org/10.1021/jacs.2c04301.

[22] L. Wei *et al.*, "NiO nanosheets coupled with CdS nanorods," *Front. Chem.*, vol. 9, 2021, https://doi.org/10.3389/fchem.2021.655583.

[23] J. W. Lee *et al.*, "Photoelectrochemical water splitting using nanostructures," *J. Mater. Chem. A*, vol. 9, no. 38, pp. 21576–21606, 2021, https://doi.org/10.1039/D1TA04829E.

[24] L. Brock and J. Sheng, "Fabrication of polymeric nanowires," *Micromachines*, vol. 11, no. 1, 2019, https://doi.org/10.3390/mi11010046.

[25] A. Al-Haddad *et al.*, "Ultrathin alumina membranes," *ACS Nano*, vol. 9, no. 8, pp. 8584–8591, Aug. 2015, https://doi.org/10.1021/acsnano.5b03789.

[26] D. Chidambaram *et al.*, "Surface pretreatments of aluminum alloy," *J. Electrochem. Soc.*, vol. 151, no. 11, 2004, https://doi.org/10.1149/1.1806393.

[27] P. J. Kelly and R. D. Arnell, "Magnetron sputtering," *Vacuum*, vol. 56, no. 3, pp. 159–172, 2000, https://doi.org/10.1016/S0042-207X(99)00189-X.

[28] H. Masuda and M. Satoh, "Gold nanodot array fabrication," *Jpn. J. Appl. Phys.*, vol. 35, no. 1B, 1996, https://doi.org/10.1143/JJAP.35.L126.

[29] P. Scherrer, "Bestimmung der Größe…," *Nachr. Ges. Wiss. Göttingen, Math. -Phys. Kl.*, vol. 1918, pp. 98–100, 1918, https://doi.org/10.1002/andp.19183610202.

[30] A. L. Patterson, "The Scherrer formula for X-ray particle size determination," *Phys. Rev.*, vol. 56, no. 10, pp. 978–982, 1939, https://doi.org/10.1103/PhysRev.56.978.

[31] G. K. Williamson and W. H. Hall, "X-ray line broadening from filed aluminum and wolfram," *Acta Metall.*, vol. 1, no. 1, pp. 22–31, 1953, https://doi.org/10.1016/0001-6160(53)90006-6.

[32] J. Zhu *et al.*, "Optical absorption enhancement in silicon nanowires," *Nano Lett.*, vol. 9, no. 1, pp. 279–282, 2009, https://doi.org/10.1021/nl802886y.

[33] L. Cao *et al.*, "Semiconductor nanowire optical antenna absorbers," *Nano Lett.*, vol. 10, no. 2, pp. 439–445, 2010, https://doi.org/10.1021/nl9036627.

[34] P. Makuła *et al.*, "Determining band gap energy," *J. Phys. Chem. Lett.*, vol. 9, no. 23, pp. 6814–6817, 2018, https://doi.org/10.1021/acs.jpclett.8b02892.

[35] A. Al-Haddad *et al.*, "Optical absorption band edge of TiO_2 nanotubes," *J. Phys. Chem. C*, vol. 119, no. 28, pp. 16331–16337, 2015, https://doi.org/10.1021/acs.jpcc.5b02665.

[36] S. Tarish *et al.*, "ZnO/ZnS core/shell nanotube arrays," *J. Phys. Chem. C*, vol. 119, no. 3, pp. 1575–1582, 2015, https://doi.org/10.1021/jp510835n.

[37] S. Tarish *et al.*, "Optical absorption band edge shift," *J. Mater. Chem. C*, vol. 4, no. 7, pp. 1369–1374, 2016, https://doi.org/10.1039/C5TC04152J.

[38] Z. Chen, H. N. Dinh, and E. Miller, *Photoelectrochemical Water Splitting*. New York, NY, USA: Springer, 2013, https://doi.org/10.1007/978-1-4614-8298-7.

[39] Z. Li *et al.*, "Tunable band alignment in Nb_3O_7F nanocrystals," *Nanotechnology*, vol. 29, no. 22, 2018, https://doi.org/10.1088/1361-6528/aab68e.

[40] K. Zhu, G. Mul, and A. Huijser, "Dye-sensitized NiO photocathodes," *Chem. Phys. Rev.*, vol. 5, no. 2, 2024, https://doi.org/10.1063/5.0170022.